GeoResJ 8 (2015) 1–13

Contents lists available at ScienceDirect

GeoResJ

journal homepage: www.elsevier.com/locate/grj

Pressurized groundwater systems in Lunae and Ophir Plana (Mars): Insights from small-scale morphology and experiments

Wouter A. Marra[a,*], Ernst Hauber[b], Steven M. de Jong[a], Maarten G. Kleinhans[a]

[a] Faculty of Geosciences, Universiteit Utrecht, Heidelberglaan 2, CS Utrecht 3584, The Netherlands
[b] Institut für Planetenforschung, German Aerospace Center (DLR), Rutherfordstraße 2, Berlin 12489, Germany

ARTICLE INFO

Article history:
Received 24 February 2015
Revised 30 July 2015
Accepted 12 August 2015

Keywords:
Mars
Outflow channel
Groundwater
Surface processes
Landscape evolution
Scale experiment

ABSTRACT

Outflow channels on Mars reveal the past presence of water, possibly released from pressurized groundwater reservoirs. We aim to improve our understanding of such outflow systems in order to better constrain past hydrological conditions on Mars. We investigate the morphology of possible pressurized groundwater outflow systems on Mars and compare them to landscape evolution experiments. These experiments show that incised channels, like the classic outflow channels, form in a last, erosional, stage in morphological development. This is preceded by the formation of sedimentary lobes due to rapid water loss by infiltration. On Mars, we observe similar morphologies related to different stages of groundwater outflow in Lunae and Ophir Plana. In the experiments, pits formed by the pressure of the groundwater, whereas the pits in the source regions of the outflow channels relate to the regional tectonic structure and are not formed by groundwater alone. Faulting, subsidence and collapse likely triggered outflow from a pressurized aquifer. This scenario is consistent with the presence of one or several cryosphere-confined aquifers from the Early Hesperian to at least the middle Amazonian. A pronounced spatial trend of larger and further developed outflow systems at lower elevations suggests that features ranging from small lobes to large outflow channels were sourced from a common aquifer or from aquifers with similar pressures. The required cryosphere indicates a cold climate and enables groundwater outflow even under atmospheric conditions unfavorable for sustained presence of liquid water.

1. Introduction

Mega-outflow channels are among the most widely discussed features that evidence former fluid water on planet Mars (e.g. [5,9,17,24,28]). These outflow channels emerge from tentative former basins (e.g. [32]), tectonic fissures (e.g. [30]), pits (e.g. [17,34]) and chaotic terrains (e.g. [31,36,49]). The most common explanation for the origin of water for these large valleys is groundwater [5] as there are no upstream drainage systems. The size and morphology of the large outflow channels suggest high-discharge events, which require a pressurized aquifer. Alternatively, lava flows have been proposed as an erosional agent for several outflow channels (e.g. [37]).

Possible groundwater pressurization mechanisms are recharge from high elevation infiltration [14,26], tectonism [25,62], volcanism [52] or aquifer freezing [61]. A confining cryosphere on top of the aquifer [14,15,35] is a viable cause for high pressure that can result in local outbursts of groundwater. In addition to groundwater outflow, temporary water buffers such as surface lakes (e.g. [17,38,64]), collapse of buried lakes [49] or subsurface reservoirs of fluid water [41] are possible causes for release of high outflow flood peaks.

The wide range of theories of outflow channel formation hinders hydrological and climatic interpretations. Therefore, an improved understanding of groundwater outflow processes offers insights into the formative conditions of outflow channels and other outflow-related morphologies. In an earlier contribution [41], we presented landscape evolution experiments on pressurized groundwater outflow and evaluated the associated processes and feasibility qualitatively using numerical modeling. Guided by these experimental insights, we focus on the morphology and identify surface features on Mars that indicate groundwater outflow to identify sources of groundwater, outflow processes and the required hydrological conditions.

First, we review our experimental results on pressurized groundwater outflow processes and resulting morphological features. Then

* Corresponding author. Tel.:+31 (0)30 253 2183.
E-mail addresses: w.a.marra@uu.nl (W.A. Marra), ernst.hauber@dlr.de (E. Hauber), s.m.dejong@uu.nl (S.M. de Jong), m.g.kleinhans@uu.nl (M.G. Kleinhans).

http://dx.doi.org/10.1016/j.grj.2015.08.001

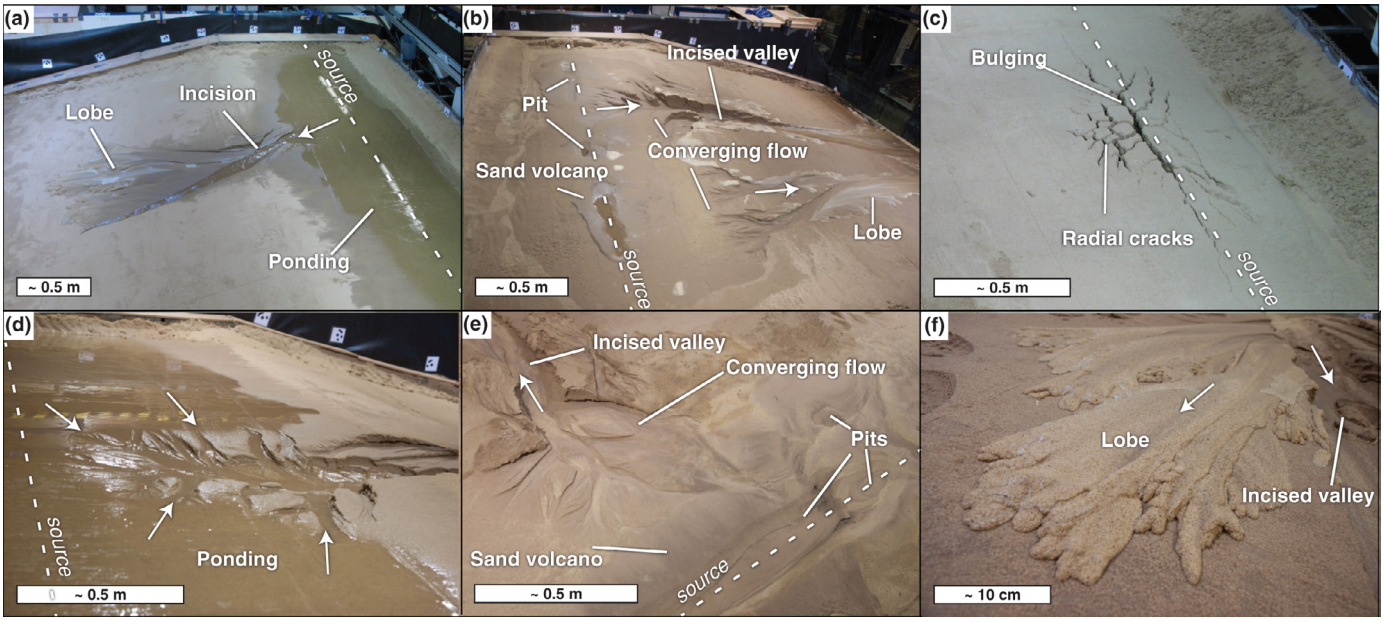

Fig. 1. Groundwater outflow morphology, photographs of the scale experiments [41]. (a) Outflow from seepage above the source area with downstream lobes and incising channel (experiment 1). (b) Outflow pits with standing water surrounded by sedimentary lobes, converging flow features and downstream valleys (experiment 2). (c) Radial cracks due to formation of subsurface reservoir moments before outflow (experiment 3). (d) Close-up of source area showing converging flow morphology and terraces in the background (experiment 1). (e) Close-up of outflow pit (lower right and upper right) with sedimentary lobe, incised valley and smaller lobes of initial outflow (upper middle) (experiment 2). (f) Close-up of sieve lobe with later incised valley in the background (experiment 1).

Table 1
Key morphological features observed in the experiments [41], formative processes in the experiment and possible processes responsible for similar morphology on Mars.

Morphological feature	Process in experiment	Experiment	Possible process on Mars	Mars
Pit	Outflow erosion	Interm. and high, Fig. 1b and e	Collapse of subsurface void	Figs. 4, 5, 7
Sand volcano	Deposition of material from pit	Interm. and high, Fig. 1b and e	Same as experiment	Figs. 5g and 7 e
Radial cracks	Creation of subsurface reservoir	High pressure, Fig. 1c	Bulging by other process	Fig. 8
Converging channels	Flow convergence in outflow region	All experiments, Fig. 1b, d, e	Same as experiment	Fig. 5
Lobate deposits	Infiltration of high-sediment concentration flow	All experiments, Fig. 1f	Same as experiment	Figs. 4, 5, 7
Incision in lobe	Early stage of incision	All experiments, Fig. 1a	Same as experiment	Fig. 5
Strong incision	Developed channel after sustained outflow	All experiments, Fig. 1b and d	Same as experiment	Fig. 6

we present our methods, study area and morphological maps of the Martian surface. We discuss selected cases, focusing on their formation, relation to other features, the chronology of events and the implications for the hydrological system and climate.

2. Groundwater outflow processes and morphology

2.1. Experimental outflow processes and morphology

We conducted a range of landscape evolution experiments on groundwater outflow processes [41]. The experiments simulated the outflow of pressurized groundwater in a 4-by-6 m sandbox, consisting of two areas: a flat area above the groundwater source where we could observe the outflow processes and a sloping area that allowed for valley formation and other downstream processes (Fig. 1). Here, we summarize the main results of these experiments and key morphological features (Table 1) to aid our interpretation of comparable systems on Mars.

The experiments were carried out with three different groundwater pressures, resulting in different outflow processes above the groundwater source. At low pressure below the lithostatic pressure but above the hydrostatic pressure, groundwater slowly seeped to the surface forming a shallow lake, which eventually overflowed. At an intermediate pressure of roughly the lithostatic pressure, fissures formed which resulted in a higher outflow discharge. Finally, at high pressure well above the lithostatic pressure, the surface bulged and cracked, and a subsurface reservoir formed that suddenly erupted causing a short high-discharge outflow event.

These different pressures produced different source morphologies. Seepage in the low-pressure experiments did not cause significant erosion (Fig. 1a). Under intermediate pressure, the outflow through fissures resulted in pits above the groundwater source due to removal of sediment, which was deposited around the pits (Fig. 1b). The bulging surface in the high-pressure experiment initially resulted in surface cracks radiating from the center of the bulge (Fig. 1c). After the collapse of the subsurface reservoir, the outflow through fissures, resulting in a similar morphology in the outflow area as the intermediate pressure experiment. All experiments ultimately carved a valley as water flowed onto the sloping section. The transition from source area to downstream valley produced a converging fan-shaped valley head in all experiments (Fig. 1d and e).

We observed two types of lobes. Firstly, there were lobes surrounding the outflow pits that were the result of sediment emerging from the pit, similar to a sand-volcano. Further downstream, we observed lobes of sediment eroded from the initial valley head that deposited due to infiltration of water, also known as sieve-deposits [44] (Fig. 1f). Such sieve-deposits are fan-shaped, being wider in downstream direction. These lobes formed in the early stages of the experiment when the downstream substrate was still dry.

As the experiments continued, the deposition of these lobes occurred further from the source and finally ceased as the area of saturated substrate extended radially from the groundwater source. The

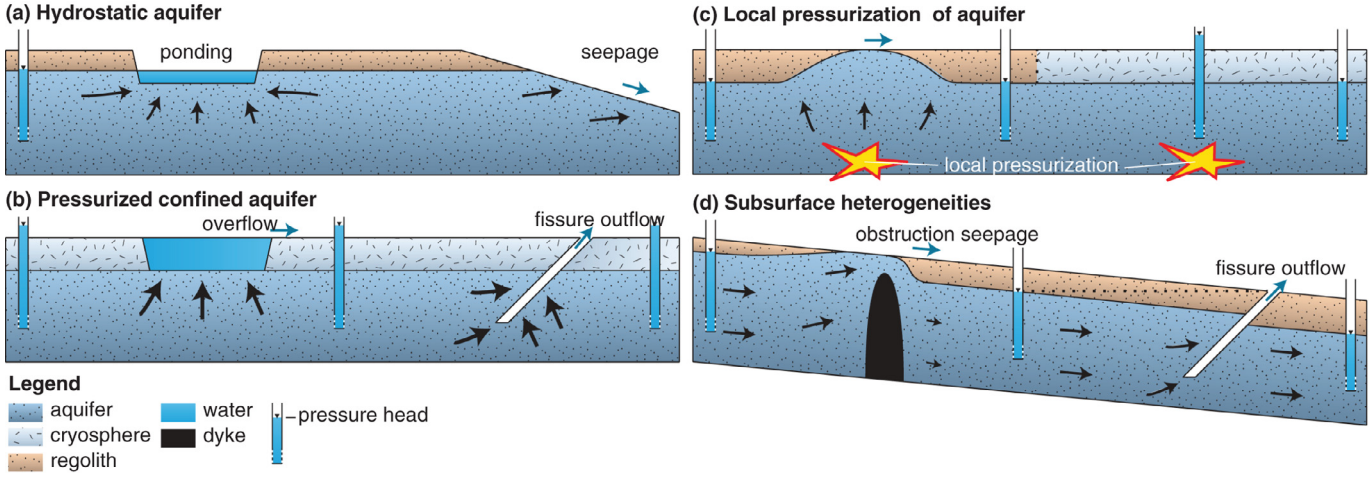

Fig. 2. Hypothesized groundwater outflow mechanisms for Mars. (a) Groundwater outflow due to seepage from a hydrostatic aquifer, resulting in ponding in a depression and outflow at slopes. (b) In case of a pressurized aquifer, depressions can overflow and outflow locations are a function of subsurface properties. (c) Local pressurization and (d) subsurface heterogeneities may alter the outflow location (in this example, outflow is the result of a disruption of regional, topographic driven, groundwater flow).

flow then continued as concentrated surface runoff which incised and formed valleys with terraces. Valley formation started at the upstream end while downstream lobes formed (Fig. 1a), and incised to the downstream end as the outflow continued (Fig. 1b and d).

2.2. Scaling experimental morphology to Mars

Landscape experiments are not direct scale models for natural systems for various reasons, mainly due to the different size and material. Nevertheless, these experiments function as analogs that show the main processes like groundwater flow, fluvial flow and sediment transport, and related patterns in the morphology, but at different relative scales (e.g. [46]). In order to apply the experimental results to the Martian surface, we first identify their similarities and differences.

A main difference between experiment and Mars is the material. Our experimental setup consisted of sand, whereas the substrate in our study area likely consists of degraded sedimentary, impact and/or volcanic material [58]. Erosion rates differ between these materials, but the general morphological patterns are similar (see discussion in [40]).

In the outflow source area in the experiments, we observed the formation of pits due to high-pressure groundwater outflow. Surrounding these pits, a part of the eroded material deposited in a similar way as a sand volcano: due to the divergence of flow out of the pit. If flow is sufficiently large, such erosional pits may also form on Mars. However, other processes may result in the formation of pits, for instance by tectonic activity, magmatic activity or karst formation (Table 1).

In the experiments, we observed lobate deposits. Important factors for the formation of lobes are initial sediment concentration and rate of water loss which reduces the carrying capacity for suspended sediment. In our experiments, sediment eroded from the outflow source formed the lobes and water loss was the result of infiltration due to flow over unsaturated substrate. In case of Mars, we expect high sediment concentrations in an early stage of groundwater outflow. Loose, weathered material in the outflow area at the surface and possible from the subsurface is picked up by the first outflow. We assume that the water from this concentrated flow infiltrates in the upper layer of the Martian regolith as such material is highly porous. Due to the low atmospheric pressure and temperature on Mars, boiling, evaporation and freezing of the surface of the flow play an additional role on Mars [6,18] that was not simulated in the experiments.

2.3. Mechanisms for groundwater pressurization and outflow on Mars

To create groundwater pressure required for outflow, we consider two mechanisms: outflow from a hydrostatic aquifer (Fig. 2a) and outflow from a pressurized aquifer (Fig. 2b). We also discuss local pressurization mechanisms (Fig. 2c) and the effect of subsurface heterogeneities (Fig. 2d).

From a hydrostatic (unpressurized) aquifer, groundwater may emerge at topographic depressions if the surface elevation falls below the groundwater table. Closed depressions at the surface result in lakes and seepage at slopes will flow down and results in valley formation by seepage erosion (Fig. 2a). In the case of seepage into depressions, the resulting lakes will not overflow if the groundwater table, and thus maximum lake level, is below the rim of the depression.

For groundwater to emerge at topographic highs or overflow closed depressions, the groundwater needs to be pressurized so that the hydraulic head is above the surface. Such regional pressurization occurs when an impermeable layer (aquiclude) on top confines an aquifer with variation in elevation (Fig. 2b). The cryosphere, a layer of frozen groundwater and regolith, is a likely candidate for an aquiclude on Mars [14]. The surface of our study area is partly covered by basalt to tens of meters in thickness (eHv in [58]). If there is limited jointing, such basalts could have a lower permeability than the underlying Noachian regolith. In that case, the basalt may have aided in the confinement of the aquifer below. In addition to a topographic gradient, the formation of the cryosphere itself may also result in elevated pressures due to volume decrease of the aquifer as the freezing water expands [61]. In case of a confined aquifer, the groundwater is released where the aquiclude is disrupted, for example at tectonic faults (Fig. 2b).

Locally, external forces can increase the groundwater head and cause localized outflow. Such forces are tectonism [25], meteor impacts [62] or magmatism. The interaction of magma with groundwater or the cryosphere cause violent eruptions of groundwater, both due to vaporization and consequent breakdown of the confining layer [12,36]. Elevated groundwater pressure in an unconfined aquifer would result in seepage above the pressure source, or contribute to the pressure in a confined aquifer (Fig. 2c).

Local subsurface heterogeneities affect groundwater outflow (Fig. 2d), these are for example impermeable dykes and faults. An obstruction of the flow by impermeable barriers like dikes (e.g. [4,7]) may locally increase the hydraulic head. Faults with a higher

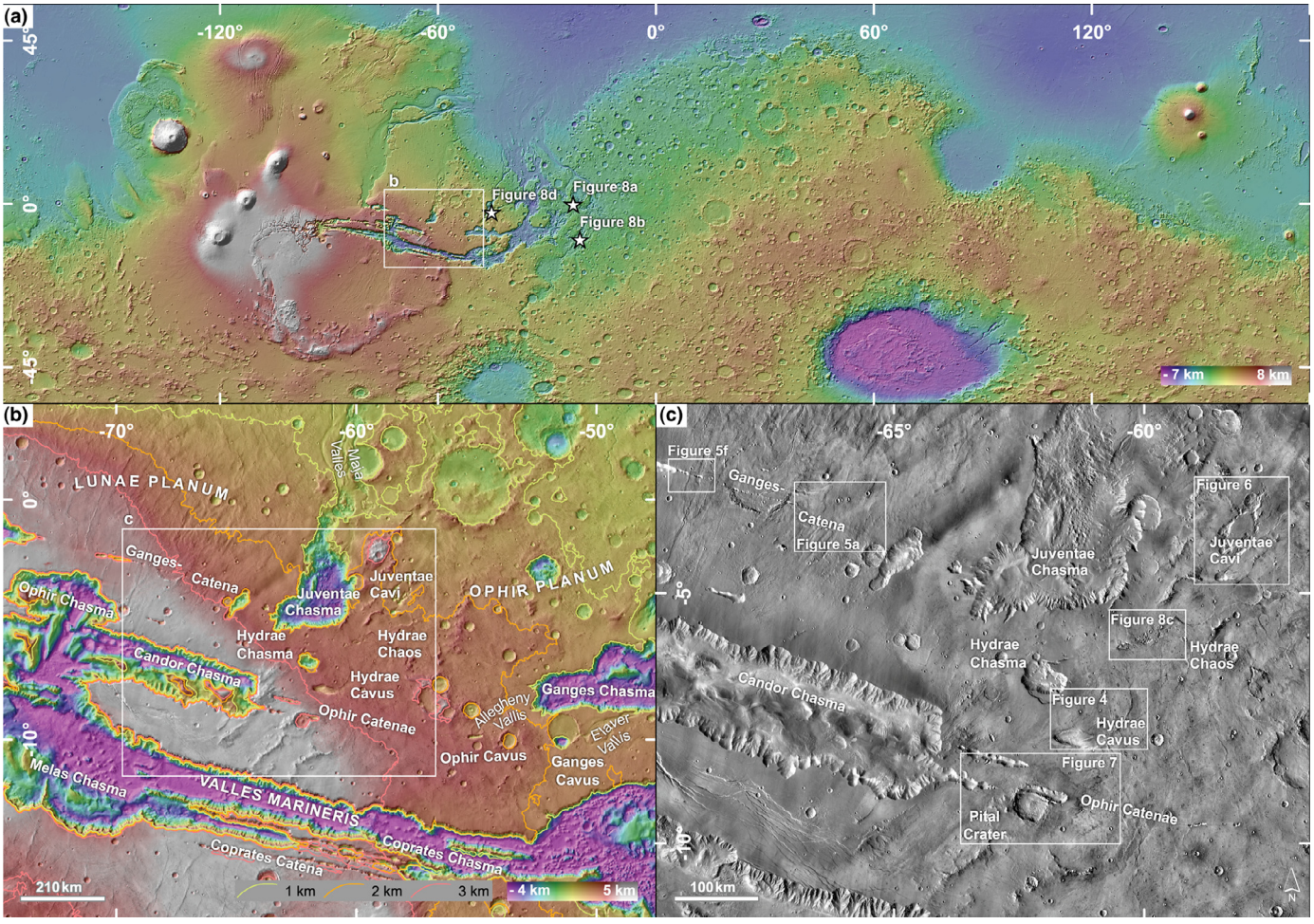

Fig. 3. Overview map of study area. (a) Colored MOLA data showing extent of panel (b) (this figure) and locations of panels (a), (b) and (d) of Fig. 8. (b) Colored MOLA data overlain by daytime THEMIS IR mosaic with 1, 2, and 3 km MOLA-contours. (c) Daytime THEMIS IR mosaic showing the extent of mapped area in Figs. 4–7 and 8c.

permeability as the regolith or zones of high permeability in the upper part of the aquifer may focus groundwater outflow. In such cases, a pressure gradient in the groundwater should be present to drive the outflow, such as a regional topographic gradient (Fig. 2d).

3. Study area and methods

We mapped several features in the southeast of Lunae Planum and western Ophir Planum, north of Valles Marineris (Fig. 3), since this area hosts several classic mega-outflow channels and possibly former lakes (e.g. [23,31,34]). This area is characterized by chasmata, pit chains and faults with a northwest-to-southwest orientation. Juventae Chasma is located at the source of Maja Valles, an outflow channel that drained towards the north-northeast [31]. The large outflow channels of Kasei Valles are located west of the studied area and the smaller outflow channels Allegheny, Walla Walla and Elaver Valles are located east (Fig. 3b, [17,34]).

The morphological maps include potential depositional features, channels, structural elements such as faults and wrinkle ridges that may have controlled groundwater outflow, and impact craters where these have important cross-cutting relations with the other features of interest. These maps are based on visible and infrared imagery and topographic data. We used 100 m/pixel Thermal Emission Imaging System (THEMIS) day- and nighttime infrared (IR) mosaics [13,20] and gridded elevation data from the Mars Orbiter Laser Altimeter (MOLA, [68]). For detailed maps we used images from the Context Camera (CTX) at 6 m/pix [39], imagery and digital elevation models (DEMs) from the High-Resolution Stereo Camera (HRSC) at 12.5 and 75 m/pix resolution, respectively [33,54], and MOLA point-data. For quantitative interpretation of features in nighttime-IR images, we report thermal inertia (TI) values, a map of which was derived from TI maps provided by the U.S. Geological Survey [21] and is shown in Supplementary Fig. S1. We dated the surface of a depositional lobe (L2, Fig. 7c) based on crater-size frequency distribution [42], see Supplementary Fig. S2.

4. Morphological mapping results

4.1. Hydrae Cavus

4.1.1. Morphology

Hydrae Cavus is a 20 by 60 km, 1600 m deep pit, 50 km southeast of Hydrae Chasma (Fig. 4a). The location of the pit coincides with wrinkle ridges of various orientations (Fig. 4c). Several of the north-south oriented wrinkle ridges continue at the pit floor (arrows in Fig. 4d). The depth and width of the pit decreases toward the east (Fig. 4a). At the rim of the pit, we observe faults parallel to the rim (Fig. 4d). Inside the pit, lobes of collapsed wall material cover a small part of the pit floor.

A 75 km long lobe which is visible as a bright area in nighttime-IR imagery extends from Hydrae Cavus (Fig. 4b). The lobe is about 50 m thick at the distal end (Fig. 4f). The lobe has slightly higher thermal inertia (TI) of 250–330 J $m^{-2}K^{-1}s^{-1/2}$, compared to its surrounding where the TI is 220–290 J $m^{-2}K^{-1}s^{-1/2}$ (Supplementary Fig. S1). This

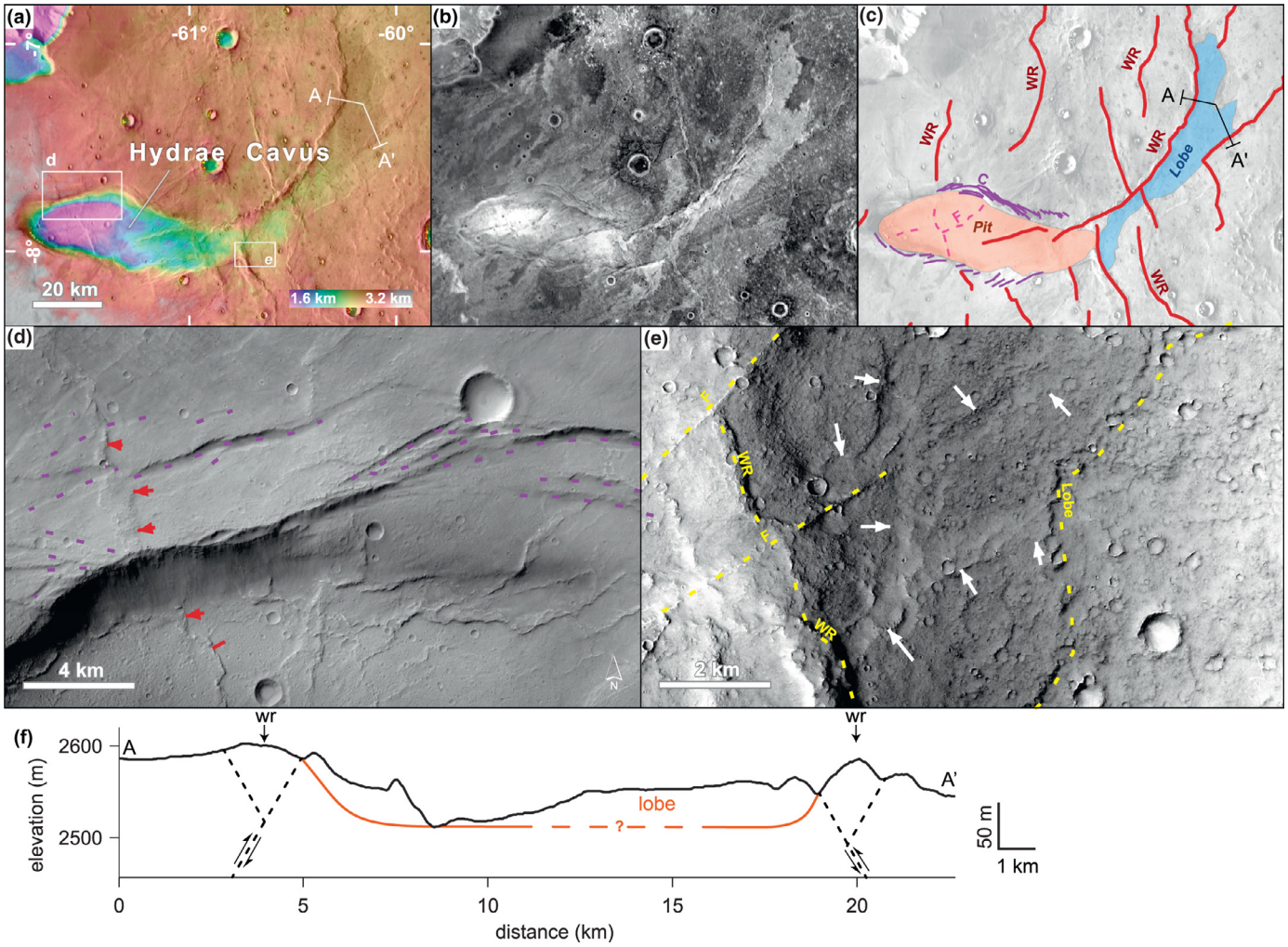

Fig. 4. Morphology of Hydrae Cavus. (a) HRSC DEM with THEMIS IR daytime mosaic, showing location of sub-figures and location of profile shown in (f). (b) THEMIS IR nighttime mosaic, (c) general morphological interpretation with pit and main lobe, WR: wrinkle ridges, F: faults on pit floor, C: collapse faults. (d) Northern rim of the pit showing collapse features (dashed lines) and wrinkle ridges (arrows). (e) Lobe emerging from wrinkle-ridge (WR), arrows indicate shallow channelized features. Subfigures (d)–(e) are CTX imagery. (f) Elevation profiles based on HRSC DEM.

lobe starts from a wrinkle ridge, east of the pit, where it shows channelized features at the surface (arrows in Fig. 4e). Two elevated wrinkle ridges confine the northeastern half of this lobe.

4.1.2. Interpretation

The faults parallel to the rim (Fig. 4d) indicate that the pit formed due to collapse and not by erosion due to groundwater outflow as was the case in our experiments. The lobe seems to originate from a wrinkle ridge or further south, but not directly from the pit itself, which further indicates that the pit itself was not excavated by fluvial erosion.

The lobe northeast of the pit could be formed by outflow of groundwater. The lobe morphology corresponds with the morphology after the initial groundwater outflow in our experiments when the water in the flow drained to the subsurface (Fig. 1f). Possible indicators of fluvial activity are the small channels at the source of the lobe (Fig. 4e). Such a lobe with small channelized features is characteristic for an early stage of groundwater outflow, the lobe consists of material eroded at the outflow source or comes from the subsurface due to turbulent flow through fissures.

Alternatively, the lobe could be formed by one or several lava flows, which typically show high TI-values. However, fluvial deposits with high sediment concentrations have a low porosity, as a high concentration of fine sediment fills the pores between larger particles. This low porosity results in a higher bulk density and lower surface area-to-volume ratio, which increases thermal inertia [47]. The reported TI-values are in the same range as hyper-concentrated flow deposits of nearby Havel Vallis [59,60], these data do not convincingly support one theory over the other.

The wrinkle ridge at the lobe apex possibly represents a deep fault in the subsurface [56]. Although such faults may not reach all the way to the surface, they may assist in channelizing groundwater flow toward the surface or be the reason for disruption of a confining layer at depth. The co-location with the pit suggests tectonism is a likely trigger of the outflow of groundwater.

4.2. Ganges Catena

4.2.1. Morphology

The easternmost part of Ganges Catena (Fig. 5) consists of a 45 km long chain of pits with individual pits between 1 and 2 km in diameter. North of these pits, we observe northeast-oriented channelized features. These features are wide next to the pits and converge farther away; they are slightly sinuous and show streamlined islands (Fig. 5d). Further northeast, the channelized morphology becomes less clear, but a bright southwest-northeast oriented feature is visible in nighttime-IR imagery which is located in a depression that gradually deepens and widens towards the northeast (Fig. 5b). This lobe

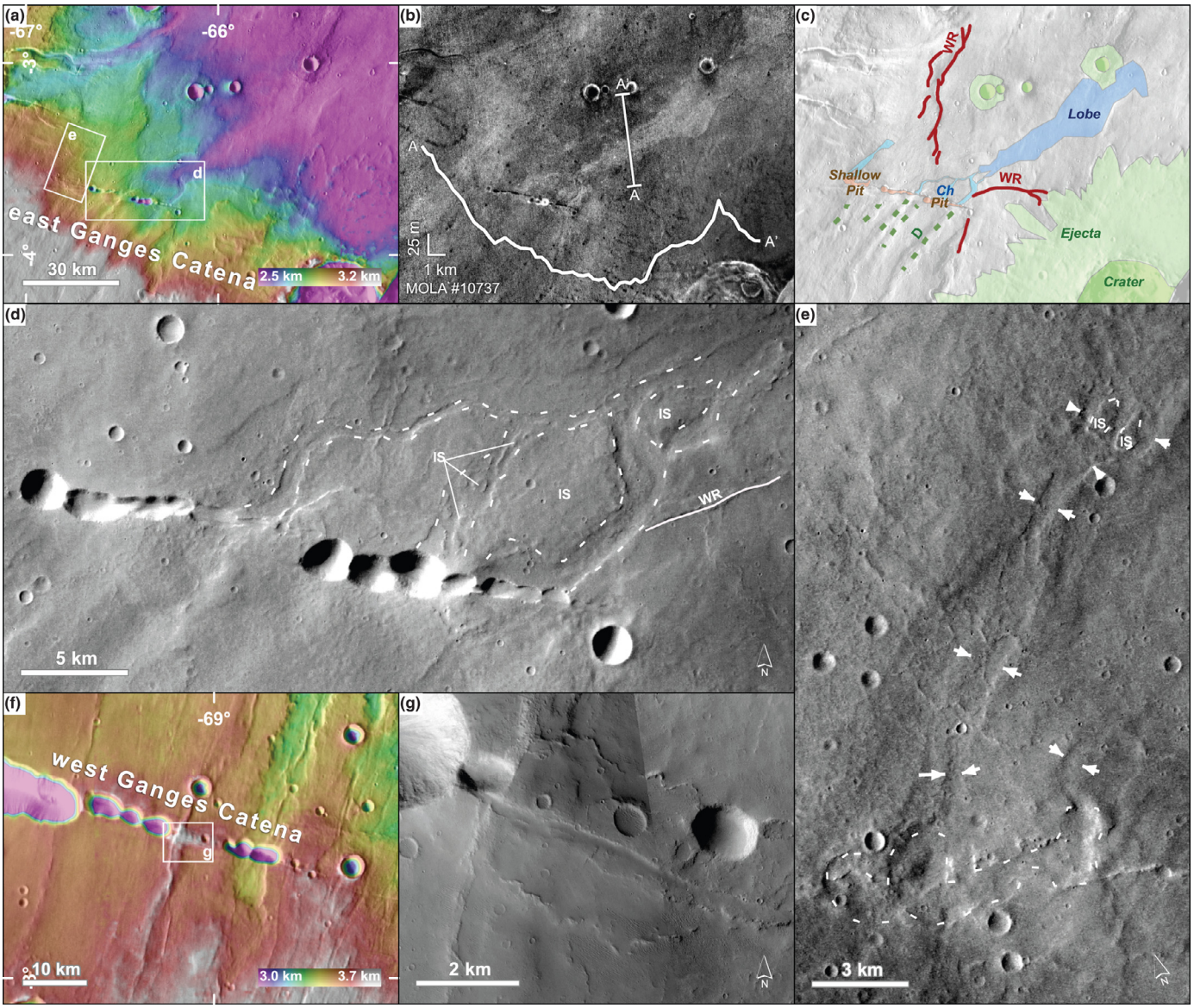

Fig. 5. Outflow features from Ganges Catena. (a) MOLA DEM with THEMIS IR daytime mosaic with location of sub-figures. (b) THEMIS IR nighttime mosaic, and MOLA elevation profile. (c) Morphological map, D: depressions, WR: wrinkle ridges. (d) Pits with channels showing outline of incises channel (dashed line), erosional islands (IS) and streamlined grooves (arrows) (HRSC image). (e) Shallow pit (outlined with dashed line) and channels (arrows indicate channel banks) with erosional islands (outlined, IS). (f) Context map with MOLA DEM and THEMIS IR daytime mosaic. (g) Lobe on both sides of a fissure enclosed by pits (CTX image).

has a TI of 135–150 J $m^{-2}K^{-1}s^{-1/2}$) and the surrounding area has a TI of 125–140 J $m^{-2}K^{-1}s^{-1/2}$ (Supplementary Fig. S1).

South of the pits, several parallel, slightly sinuous southwest-northeast oriented depressions are present, with depths of about 50–100 m (Fig. 5a). The channels north of the pit chain align with these depressions.

Shallow pits exist west of the pits described above. Northeast of these pits, we observe a small northeast-oriented channel which widens downstream and features streamlined islands (Fig. 5e). Further west in Ganges Catena, we identified a fissure that aligns with the entire catena, but has no pits. A lobe without channelized morphology surrounds this fissure (Fig. 5g).

4.2.2. Interpretation

The channels appear as fluvial landforms based on the occurrence of incised channels and streamlined islands. The lobe-shaped feature north of the pits could either be a depositional lobe or is the result of fluvial erosion that revealed a different underlying material. Elevation data show that this feature corresponds to a topographic depression with no clear deposit, which shows the bright feature with elevated TI-values likely represents material excavated by erosion (Fig. 5d).

The channels that start at the pit chain feature well preserved fluvial morphology that does not exist south of the pit chain. Furthermore, the first part of the channel just north of the pit starts wide and narrows in downstream direction (Fig. 5d), similar to the morphology downstream of the source in our experiments (Fig. 1b and e). This morphology indicates converging flow from a wide source into a channel.

The depressions south of the pits are slightly sinuous, but still relatively straight compared to the channels north of the pits. These depressions do not show fluvial features, in contrast to the channels north of the catena. These depressions could be tectonic in origin or represent degraded fluvial channels. In case of a tectonic origin, they may be the result of collapse due to groundwater flow to the

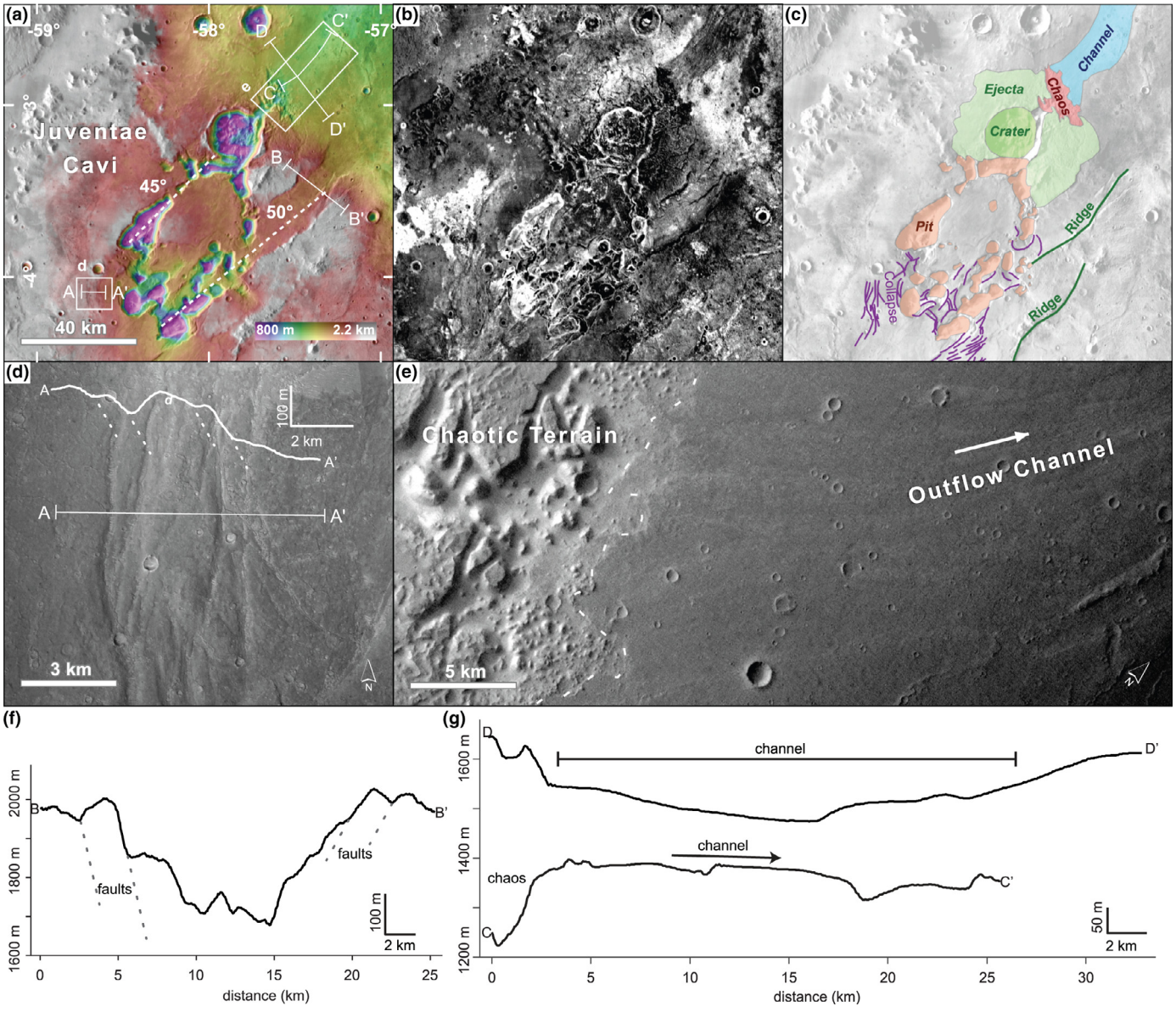

Fig. 6. Juventae Cavi and associated outflow channel. (a) HRSC DEM with THEMIS IR daytime mosaic, showing location of subfigures and profiles. (b) THEMIS IR nighttime mosaic, (c) map showing main pits (orange), chaotic terrain (red) with channel (blue), main craters with ejecta (green), collapse features outside of the main pits (purple) and ridges (green). (d) Faults parallel to a pit rim (CTX) with HRSC elevation profile. Dashed lines in profiles represent faults. (e) Chaotic terrain and channel, arrow indicates inferred flow direction (HRSC). (f) HRSC elevation profile of depression. (g) HRSC elevation profile of chaos and channel. (For interpretation of the references to color in this figure legend, the reader is referred to the web version of this article.)

catena (e.g. [51]). In this case, the orientation of these depressions is indicative for a southwest-to-northeast directed groundwater flow direction. If these depressions represent fluvial channels, they existed before the formation of the catena, which also explains the presence of the depression north of Ganges Catena.

The smaller pit and channel we observed has a similar morphology as the larger channel described above. The channel emerges from a small pit, has streamlined islands upstream, converging flow next to the pit and widening flow further downstream (Fig. 5e). The relation between channel size and pit size suggests a relation between the two. The larger pit may be an easier pathway for groundwater outflow or outflow triggered by collapse could cause this relation. In either case, there is a strong link between the tectonic structure and groundwater outflow.

The lobe at west Ganges Catena surrounding the fissure corresponds with the morphology at the outflow source in the experiments (Fig. 5g). The absence of incised features indicates a possible pristine outflow that might have been present at other locations, too, but subsequent pit formation or sustained outflow removed these features elsewhere.

4.3. Juventae Cavi

4.3.1. Morphology

Juventae Cavi is an area 200 km east of Juventae Chasma of about 100 km in diameter with pits of various sizes and depths up to 1400 m (Fig. 6). Some of the pits have a circular outline in plan-view, and many pits of different sizes coalesce into complex shapes. The orientation of the chains of pits and the ridges and troughs just northeast of the cavi is between N45° and N50° (Fig. 6a). The pits show multiple nested rims and normal faults that are oriented parallel to the rim of the pits (Fig. 6d).

Northeast of the pits, we observe a 1.5 km wide and 300 m deep depression with a N50° orientation (Fig. 6a). The walls of this depres-

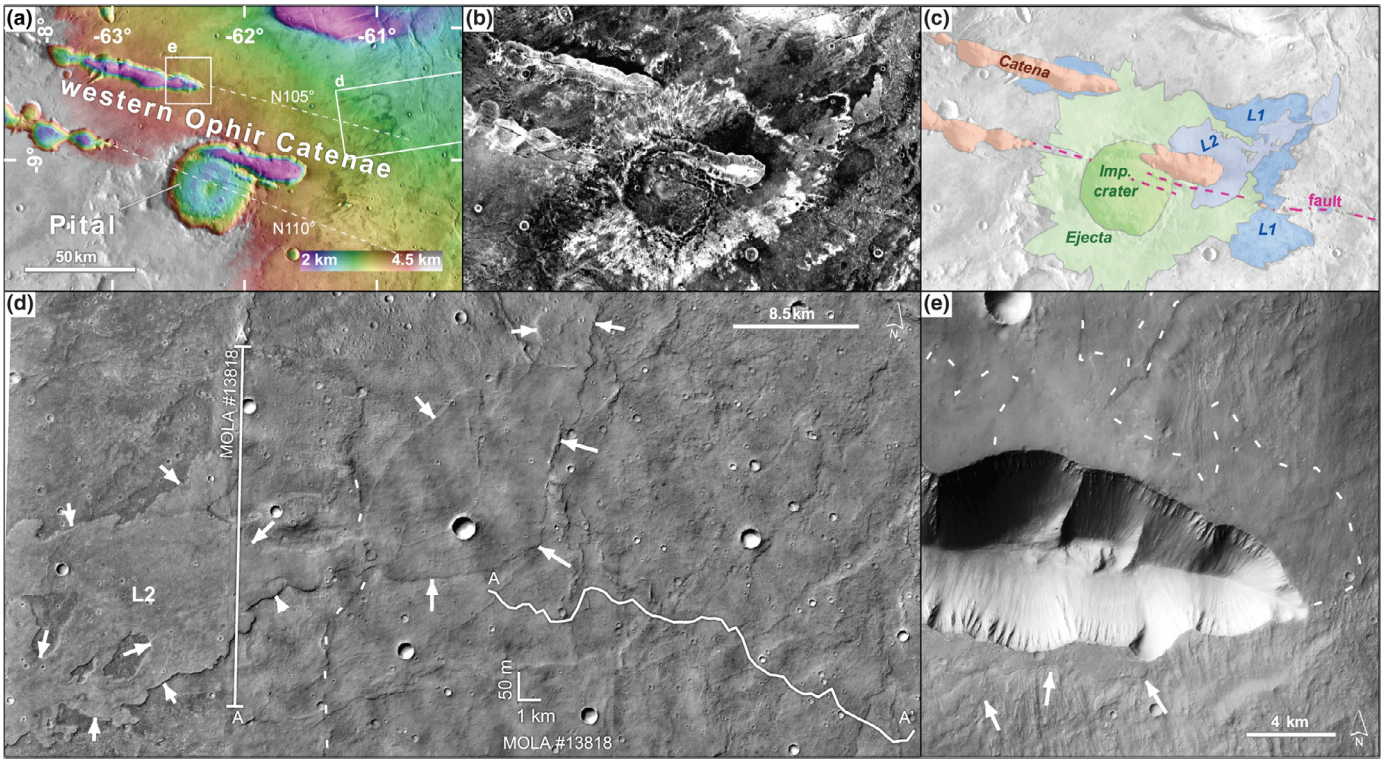

Fig. 7. Lobes around western Ophir Catenae. (a) HRSC DEM with THEMIS IR daytime mosaic, showing location of subfigures. (b) THEMIS IR nighttime mosaic, (c) morphological map. (d) Lobe extending to the northeast indicated with arrows, dashed line shows extent of older lobe, inset shows MOLA elevation profile. (e) Small lobe extending to the south of an elongated pit indicated with arrows and lobe extending to the north of that pit indicated with a dashed line.

sion show dislocated blocks, indicative for collapse of this depression (Fig. 6f).

A chaotic terrain of 20 by 8 km, a depth of 200 m and knobs up to 1 km in diameter is present northeast of the cavi. In the northeast, the landscape sharply changes to a much flatter terrain (Fig. 6e and g). At this transition, small incisional features are present and the entire area has straight linear grooves running in northeastern direction. This flatter terrain is about 20 km wide and is located in a depression that is about 100 m deep.

4.3.2. Interpretation

The presence of multiple ridges and faults on the sides of the pits and depressions in this area indicates a formation by collapse (Fig. 6d and f). The strong alignment of pits and depressions indicates a tectonic origin of Juventae Cavi, which may represent an early stage of chasmata formation like the nearby Juventae Chasma.

The channel that emerges from the chaotic terrain northeast of the cavi is likely a fluvial feature created by groundwater outflow. This channel starts at the chaotic terrain and has grooves parallel to the inferred flow direction to the northeast (Fig. 6e), which we interpret as scour marks. The orientation of this channel is the same as the pits and depressions, which indicates this channel occupies a structurally controlled depression here. The erosional grooves indicate high-energetic flow and we observed no depositional features. Such morphology is similar to the erosional channels that formed in our experiments after sustained discharge (Fig. 1e); as depositional features corresponding to early outflow stages were eroded. The location next to the cavi and the alignment with tectonic features suggest a link between tectonism and groundwater outflow.

4.4. Ophir Catenae

4.4.1. Morphology

At western Ophir Catenae (Fig. 7a), several catenae are present, as well as faults with the same N105° to N110° orientation. One of these pits joins with Pital crater. This crater has an ejecta-blanket that is visible as bright radial streaks in the nighttime-IR image (Fig. 7b). The ejecta overlays lobate features which are visibly by their very bright edges in nighttime-IR (L1 in Fig. 7c).

A smooth-textured area, dark in nighttime-IR, surrounds the eastern edge of the pit that intersects Pital crater (Fig. 7d). This morphology extends in northeastern direction as a smooth lobe (L2) that appears bright in nighttime-IR, has sharp edges and overlays the ejecta-blanket and lobe L1 (Fig. 7b and c). Lobe L2 is about 50 m higher than its surrounding (Fig. 7d). The TI-values of the distal part of the lobe are 250–280 J $m^{-2}K^{-1}s^{-1/2}$, its immediate surroundings 200–230 J $m^{-2}K^{-1}s^{-1/2}$ (Supplementary Fig. S1).

Northwest of the crater, we observed a 75 km long, 10 m wide elongated pit chain, surrounded by lobate features (Fig. 7e). These lobes align with the catena, have a smooth surface and overlay the rough impact ejecta. The lobe extends about 1–2 km to the south of the pit and up to 5 km to the north.

4.4.2. Interpretation

Lobe L2 shows a fingered pattern at the edges (Fig. 7d and e), similar to the sieve-lobes formed in our experiments corresponding to pristine groundwater outflow (Fig. 1f). However, this morphology may also be the result of lava flows as well. The height of the deposit of 50 m and the sharp edges of the lobe argue in favor of a lava flow. However, the sedimentary lobes in our experiments had also steep edges (Fig. 1f), which prohibits a definite interpretation. Likewise our interpretation of the lobe near Hydrae Cavus (Section 4.1), the TI-values of lobe L2 do not unambiguously favor any of the two hypotheses.

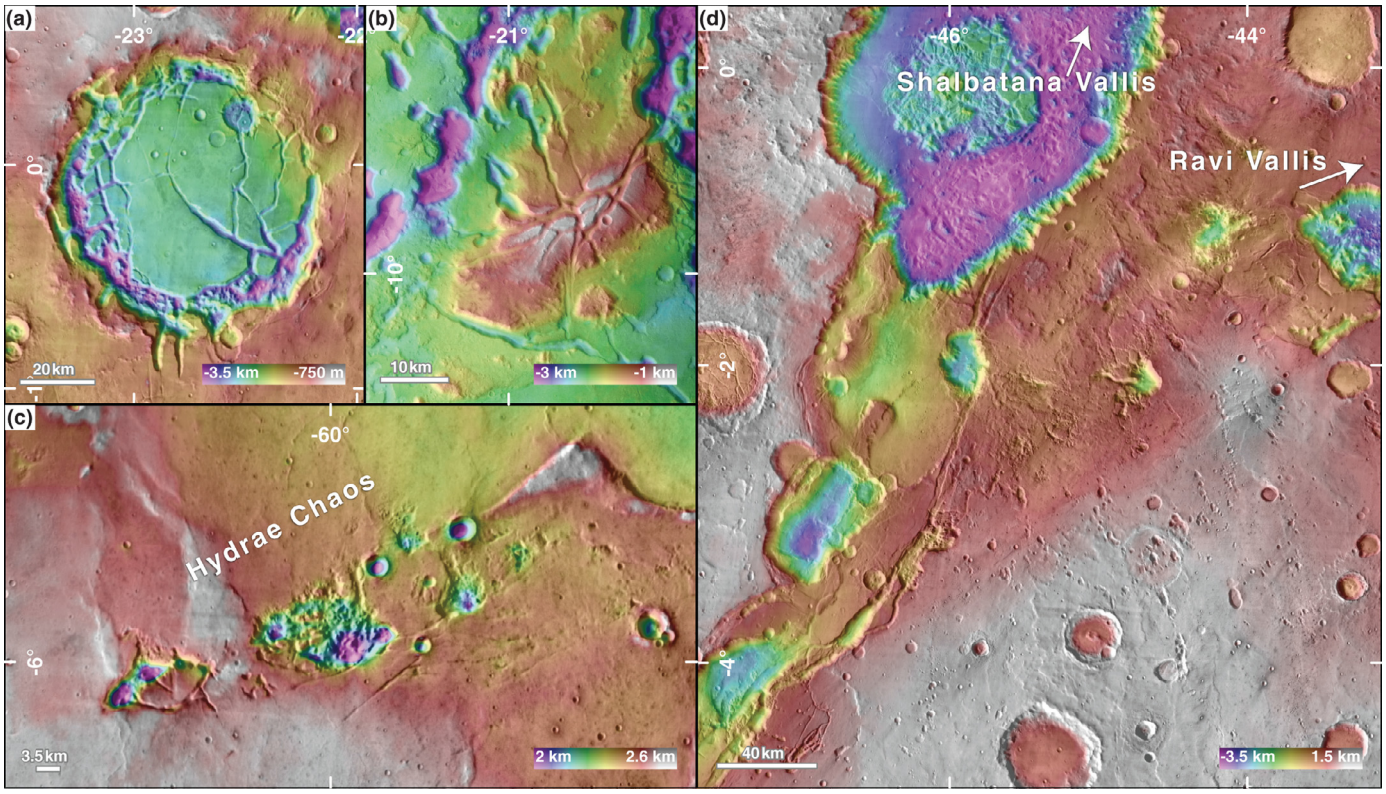

Fig. 8. Fractured features similar to experimental morphology (locations of panels shown in Fig. 3). (a) Floor-fractured crater (THEMIS IR daytime mosaic and HRSC Dem). (b) Fractured rise in Margaritifer Chaos (HRSC image and DEM). (c) Hydrae Chaos, several chaotic terrains without outflow features (THEMIS daytime IR mosaic and MOLA DEM). (d) Area upstream of Ravi Vallis (Northeast of this image), and Shalbatana Vallis (North of this image) with fractures and depressions (THEMIS daytime IR mosaic and MOLA DEM).

Pital crater and its ejecta are older than the formation of the intersecting pit, as the crater rim continues on the northern edge of the pit (Fig. 7a). The oldest feature here is lobe L1 (Fig. 7c) which is intersected by all other features. This lobe might be part of the large ejecta blanket as it has a similar radial orientation. The lobe emerging from the pit (L2, Fig. 7c) overlays the impact ejecta. Furthermore, this lobe cannot be younger than the formation of the pit to its current size as the fluid forming these lobes would have flown into the crater and not over the rim. Therefore, we associate these lobes with an early stage of the formation of the catena. Further collapse forming the pits took place after the deposition of the lobe. We dated lobe L2 (Fig. 7c, which has a crater age of 1.23 Ga (±0.23 Ga)), which is around the early/middle Amazonian boundary (Supplementary Fig. S2, Neukum chronology system, [29,42]).

4.5. Fractured features

4.5.1. Morphology

Several features on Mars have a similar morphology as the fractures observed in our high-pressure experiment (Fig. 1c). For example, floor-fractured caters (FFC) are present in Xanthe Terra [53]. The fractures in these FFC show different patterns, but cracks are often concentric and concentrated at the edges of the crater with some radial fractures running across the crater. In some cases, the edge is lower than the center of the crater (e.g. Fig. 8a). Slightly different is a fractured mount in Margaritifer Chaos (Fig. 8d). This mount is 8 to 20 km in diameter and 1 km higher than the surrounding. The fractures are mainly radial to the center of the mount.

Close the features described in the previous sections is Hydrae Chaos, which consist of several aligned chaotic terrains with no outflow features of a few to 20 km in size (Fig. 8c). These chaotic terrains are located on an arc parallel to Juventae Chasma, connecting Juventae Cavi and Hydrae Chasma. Upstream of the outflow channels Shalbatana and Ravi Valles, depressions of various sizes and fractures are present. These fractures exist in an area about 150 km across (Fig. 8d). Furthermore, there is an FFC in this area and there are chaotic terrains at the sources of the valleys.

4.5.2. Interpretation

The observed fractured features show a resemblance with the morphology of the high-pressure experiment where the surface bulged before groundwater outburst and subsided afterwards generating radial and concentric fractures, respectively. The fractured morphology upstream of Ravi Valles has a similar alignment as the experiments where the outflow took place at the side the bulged area, which is also the expected behavior of such systems on Mars [41]. Alternatively, the outflow at Shalbatana and Ravi may relate to groundwater flow from a lake in Ganges Chasma, just south of the area shown in Fig. 8d [8,10,51]. In that case, the pits and fractures upstream of these valleys are the result of collapse of the groundwater pathways. However, groundwater flow that is sourced from a lake would not be pressurized, which seems inconsistent with the chaotic source areas and high discharges responsible for Shalbatana and Ravi Vales (e.g. [36]).

These cases show no conclusive evidence for the subsurface processes responsible for the fractures. If we assume an aqueous origin of these features, this could explain both the fractures and the outflow in case of Ravi Vallis. In the cases without outflow, the water either drained back to the subsurface, leaving the cracks but not the bulge, or froze, resulting in both the cracks and bulge still being there. Magmatic features such as sills [43] could produce the same morphology and trigger the outflow of groundwater. However, a subsurface aqueous reservoir could explain the extreme high discharges for large outflow channels [41].

Hydrae Chaos may represent an intermediate stage of chasma or catena formation. These chaotic terrains align with collapsed fea-

tures, but show no signs of collapse. In Ganges Catena, the pits align with single fractures which could be the first stage of collapse, which is followed by a chaotic structure and then by collapse into a pit.

5. Discussion

The features described in this study are similar to the different stages in the development of groundwater outflow observed in our experiments. We observed lobes at Hydrae Cavus and Ophir Catenae (Figs. 4 and 7), channels emerging from Ganges Catena (Fig. 5) and a fully incisional channel that emerges from a chaotic terrain at Juventae Cavi (Fig. 6). This morphological sequence is similar to the sequence we observed in our experiments, which ranges from deposition of sedimentary lobes due to infiltration of water to an incising channel (Table 1). Alternatively, lobate features from Ophir Catenae likely formed by lava. In Section 5.1, we discuss the arguments for an aqueous versus lava origin of these features.

Previous studies showed outflow channels that reached the last, fully incisional stage, for example Maja, Allegheny and Elaver Valles [17,31], and lobate features with a possible groundwater origin [66]. Our experimental results now link these different types of features and indicate they can form from a similar hydrological system, but represent different stages in their development. In Section 5.2 we discuss, the chronology of events and in the remainder of the discussion we reconstruct the hydrological system responsible for the outflow features described in this study and surrounding area.

5.1. Groundwater versus lava flow

We described channels and lobes that are possibly related to groundwater outflow. An alternative interpretation is that these are formed by lava; similar morphology has been attributed to mudflows with high sediment concentrations or lava flows of low viscosity [66]. The strongest indicator for fluvial flow are the channels and erosional features at east Ganges Catena (Fig. 5) and the incised channel near Juventae Cavi (Fig. 6).

The lobes that emerge from Hydrae Cavus (Fig. 4) and west Ophir Catenae (Fig. 7) appear similar to the depositional lobes from our experiments, but their origin remains ambiguous. We have interpreted the lobe from Hydrae Cavus (Fig. 4) as fluvial, based on the channelized apex, although this is not conclusive evidence. The lobe from west Ophir Catenae (Fig. 7) has characteristics of a lava flow, judging on the height of this deposit. In both cases the TI-values are elevated, but do not discriminate lava from high-concentrated flow deposits. Thermal inertia (TI) values for lava flows are high and presumably higher that sedimentary deposits. However, hyperconcentrated flows may also have elevated TI-values as filling of voids between large particles by fine sediment decreases the porosity [47,59,60]. In either case, the close similarity of these lobate features warrants careful consideration of such morphology.

We found no conclusive evidence for a possible aqueous origin of the fractures described here (Fig. 8), which all could be related to volcanism. However, similar features formed in our experiments solely by groundwater, which needs to be considered as a possible mechanism for such features. Similarly, we cannot rule out a lava origin for the observed lobes based on their morphology alone. But our experiments show that different types of lobes can form solely by groundwater outflow, and the association of other outflow features that more clearly have an aqueous origin, points in the direction of the water outflow hypothesis and shows this to be a viable, parsimonious explanation for the observations.

5.2. Chronological framework

The outflow features described in this paper occur in volcanic plains formed in the early Hesperian (eHv in [58]), these outflow features are therefore of early Hesperian age or younger. Similarly, most circum-Cryse outflow channel activity peaked in the Hesperian, e.g. Kasei Valles (3.4 Gyr, [45]), although outflow events continued in the Amazonian [45,50]. Besides the outflow channels, lakes likely existed in this region in the early Hesperian (e.g. [23,38]).

Important for this region is the formation of Valles Marineris, which took place sometime during the late Noachian to the early Hesperian [2]. After the formation of the main Valles Marineris through, the nearby chasmata likely continued to form since these cut the eHv unit [58]. Faulting in the region likely continued until and in the Amazonian [55]. Lobe L2 from western Ophir Catenae (Fig. 7c) formed around the transition from the early to the middle Amazonian (1.23 Ga $\pm$ 0.23 Ga, Supplementary Fig. S2). The final shape of the pit from which this lobe emerges was likely attained after the formation of the lobe, suggesting tectonic activity in this region in the early/middle Amazonian, which is in agreement with [55].

There is a strong link between outflow events and tectonic activity. The source areas of the outflow channels and smaller outflow features described here are in most cases tectonic features. This link is further illustrated by a temporal agreement: the outflow activity peaked in the early Hesperian which coincides with the formation of Valles Marineris and later outflow events were lower in outflow magnitude which corresponds with the presumed diminishing tectonic activity. Furthermore, previous evidence for the presence water in the form of lakes in Candor and other ancestral chasmata of Valles Marineris in the early Hesperian (e.g. [23,38]) further illustrates the link between aqueous features and tectonic structures.

5.3. Aquifer pressurization

Outflow channel activity was concentrated in the Hesperian, but continued throughout the Amazonian [50,63]. Early outflow events at Ophir and Lunae Plana in the Hesperian before the formation of Valles Marineris could be the result from recharge at higher elevation in Tharsis [27] and requires a confining layer, which we assume to be the cryosphere [14,15]. Alternatively, Carr [11] explained the high outflow locations to be sourced by groundwater flow from the polar ice caps, in agreement with the model of Clifford & Parker [15], with additional pressurization from volcanic activity or freezing of the cryosphere. However, the outflow locations are in closer agreement with recharge from Tharsis [28].

Amazonian outflow events had a lower outflow discharge (e.g. [63]), which agrees with the modest outflow from Ganges Catena (Fig. 5) in the Earle/middle Amazonian age. The outflow here and at other Amazonian outflow sites (e.g. [50]) took place after the opening of Valles Marineris, and after a possible disconnect between the Tharsis source area. This implies one of the following scenarios: (1) early outflow events did not release all groundwater pressure, which can be explained by closure of the cryosphere seal during the outflow event (e.g. [3]) or (2) there was re-pressurization of residual groundwater. Furthermore, this requires a confining layer at the floor and walls of Valles Marineris to prevent the loss of groundwater. Besides a cryosphere, vertical dykes could assist in comparting the aquifer.

Tectonism could result in elevated groundwater pressure (Fig. 2b and c, [19]), which is viable mechanism for our study area as the outflow features we show in this study have a strong relation to the tectonic structure as they emerge from fissures, pits and a chaotic terrain. The outflow source areas align with other pits, catenae and chasmata in the region which correspond to the regional tectonic extensional system [1,67]. In case of Hydrae Cavus, the outflow lobe emerges from a wrinkle ridge next to the pit and in the case of Juventae Cavi, an area with collapse features is next to the source chaos

of an outflow channel. These systems are similar to the Maja Valles, where Juventae Chasma is a large area of subsidence just next to the outflow source Baetis Chaos [31]. We hypothesize that especially the collapse contributes to locally elevated groundwater pressures.

Volcanic dykes in the subsurface could act as a barrier for groundwater flow (Fig. 4) and deflect groundwater flow along faults [7]. In these cases, groundwater outflow locations are controlled by subsurface intrusive bodies and fault zones. As volcanic dykes are observed close our study area [22], the outflow locations are likely affected by their presence.

5.4. Outflow triggers

Tectonism is a likely candidate to break the confining layer of an aquifer and trigger outflow. We observed outflow directly from fissures (Fig. 5g), but also from pits aligned with such fissures (Figs. 5a and 7), which is similar to the source of Elaver Vallis ([34], their Figs. 8 and 9d). In the latter cases, the sharp morphological transitions from the pit to the valley suggest that the outflow already occurred before the pit reached its final morphology and likely relates to the initial fissure formation. Later collapse resulted in the formation of the entire pit, possibly aided by dissolution of acidic groundwater infiltrated over Tharsis [57]. Furthermore, we observed shallow pits with a small channel (Fig. 5e) and deeper pits with larger downstream channels (Fig. 5d). This trend in size of the source pits and outflow features continues for Allegheny, Walla Walla and Elaver Valles [17,34] and is further evidence for an outflow trigger by tectonism.

Alternatively, subsurface magmatism may also have triggered groundwater outflow (e.g. [52]). Dykes exist in the walls of Coprates Chasma [22], although these are of Noachian age and older than the outflow events. The formation of such dykes may disrupt the cryosphere, and older, existing, dykes may influence the groundwater flow patterns.

5.5. Regional hydrology

Several outflow channels exist near the features we mapped in this paper, with similar tectonically influenced source areas. These are Maja Valles to the North [31], and Elaver, Walla Walla and Allegheny Valles to the East (Fig. 3b, [17,34]). Together with the features mapped in this paper, there is a trend of higher outflow discharges at lower elevation. The smaller features described in this study originate at MOLA-elevations of about 3 km (Fig. 3b). Allegheny Vallis and Walla Walla originate at about 2.2 km, Elaver Vallis at 1.8 km and Maja Valles at about 1 km. The discharge estimate for Allegheny, Elaver and Maja Valles are 0.7–3 $\times$ 10^6, 20–35 $\times$ 10^6 and 100–1000 $\times$ 10^6 m^3/s, respectively [16,17,31]. The discharges at Elaver Vallis is likely higher than the groundwater outflow flux due to the presence of a lake in Morella Crater prior to outflow through the valley [16].

The strong trend of larger groundwater outflow features at lower elevations may result from a similar groundwater head for the entire region and suggests one regional aquifer or several with similar pressure. Lower elevation corresponds to higher groundwater head relative to the surface, and in turn higher outflow discharge (Fig. 9). We assume an aquifer with a groundwater head of 4 km (above MOLA datum). This assumption is not based on evidence at this point, but serves the following thought experiment. In natural systems, pressure heads likely differed over time. This head of 4 km corresponds to an overpressure of groundwater head ranging from 1.2 km at our small outflow features to 3.0 km at the source of Maja Valles (Fig. 9). In addition, such regional aquifer is a possible source of water for lakes that existed in Valles Marineris and surrounding chasmata and catenae, depending on the actual head and when aquifer existed (e.g. [23,48,65]).

We hypothesize that outflow of groundwater occurred from an aquifer, likely fed and pressurized by recharge from Tharsis in the Hesperian. Outflow was triggered by the extensional tectonism in this region leading to faults through the cryosphere, or by volcanic disruption of the cryosphere. This aquifer did not lose all pressure in early outflow events, or residual groundwater was re-pressurized for later events. Re-pressurization could be local, for example due subcryosphere volcanism or by surface collapse. Volcanism is in agreement with the basaltic material that covers the region. Pressurization by collapse of chasmata or catenae relates to the regional extensional tectonism. A local source of pressure can explain Amazonian outflow events after the formation of Valles Marineris, which likely restricted recharge from Tharsis. A confining cryosphere that is the necessary condition for pressurized groundwater indicates a cold climate. The mechanism of pressurized aquifers would allow for liquid groundwater and cause a range of outflow features, even if the surface conditions did not sustain the presence of liquid water at the surface for a long time.

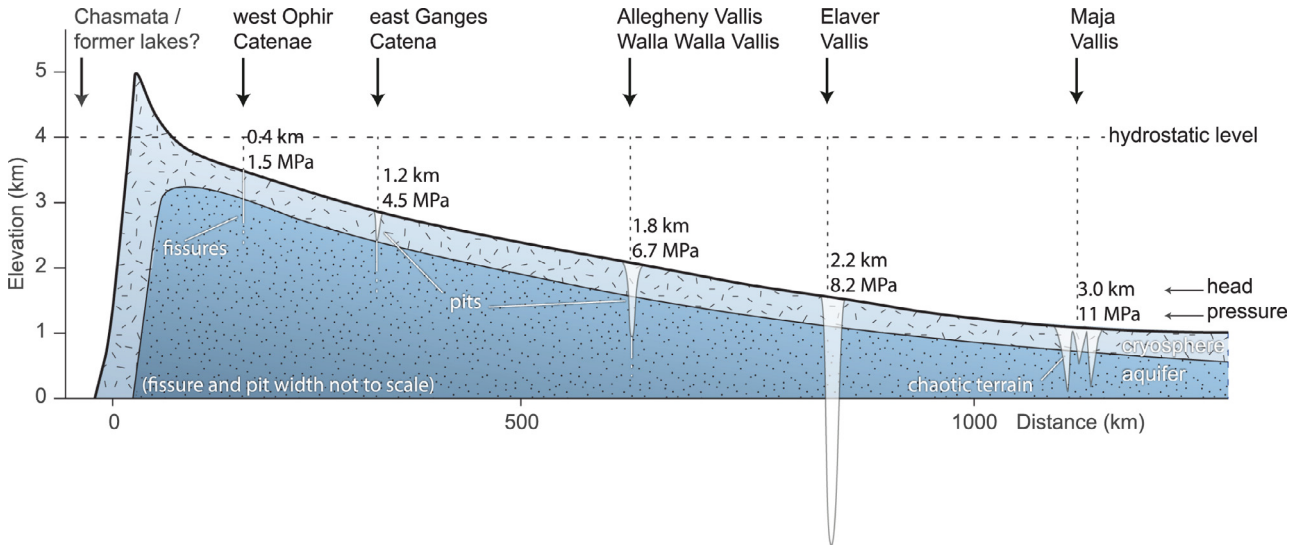

Fig. 9. Schematic cross-section from Valles Marineris showing the location of different types of outflow features. Values correspond with groundwater head above surface and corresponding pressure in case of a confined aquifer with a pressure head at 4 km, which is equivalent to a source lake at that elevation. Elevation is bases on MOLA data.

6. Conclusions

Based on experimental analogs, we identified possible groundwater outflow features on Lunae Planum and Ophir Planum that are novel indicators of pressurized groundwater outflow events. These are lobes from Hydrae Cavus and Ophir Catenae, channels emerging from Ganges Catena and an incised outflow channel from a chaos area next to Juventae Cavi. Such morphological features represent different stages of development, similar to the development we observed in our pressurized groundwater outflow landscape evolution experiments. The origin of the lobes is ambiguous as lava flow produces similar features, but the channelized features and other contextual information are possible indicators of groundwater outflow.

In addition, we observed several fractured surfaces including floor-fractured craters and fractured rises that show resemblance to the experimental morphology related to groundwater-induced flexure. Although similar to the experimental morphology, their origin is uncertain due to the absence of related fluvial features.

A regional trend of larger outflow features at lower elevations suggests that a pressurized regional aquifer confined by the cryosphere was the source for a range of outflow features, channels and possibly former lakes in the region. This aquifer existed in the Early Hesperian and was likely fed by recharge from Tharsis before the opening of the Valles Marineris troughs. Later outflow can be explained by the continued presence of pressurized groundwater or by local re-pressurization of residual groundwater. Tectonism in this region could have caused both groundwater pressurization and disruption of the cryosphere. These hydrological scenarios indicate a climate cold enough for cryosphere development, and could occur even if climate conditions were incapable of sustaining liquid surface water.

Acknowledgments

We acknowledge Thomas Platz (FU-Berlin) and Joana Voigt (DLR) for providing the crater counts and ages. We are grateful for the valuable comments by two anonymous reviewers. This work was part of the Ph.D. research of W.A.M., supported by NWO grant ALW-GO-PL/10-01. Maps were made by W.A.M. and discussed by all co-authors; interpretation by W.A.M., E.H. and M.G.K.; W.A.M. wrote the paper with input from all co-authors. The data used is provided in Supplementary Table S1.

Supplementary material

Supplementary material associated with this article can be found, in the online version, at 10.1016/j.grj.2015.08.001.

References

[1] Andrews-Hanna JC. The formation of Valles Marineris: 1. Tectonic architecture and the relative roles of extension and subsidence. J Geophys Res 2012;117:1–18. doi:10.1029/2011JE003953.
[2] Andrews-Hanna JC. The formation of Valles Marineris: 3. Trough formation through super-isostasy, stress, sedimentation, and subsidence. J Geophys Res 2012;117:E06002. doi:10.1029/2012JE004059.
[3] Andrews-Hanna JC, Phillips RJ. Hydrological modeling of outflow channels and chaos regions on Mars. J Geophys Res 2007;112:E08001. doi:10.1029/2006JE002881.
[4] Babiker M, Gudmundsson A. The effects of dykes and faults on groundwater flow in an arid land: the Red Sea Hills, Sudan. J Hydrol 2004;297:256–73. doi:10.1016/j.jhydrol.2004.04.018.
[5] Baker VR, Milton DJ. Erosion by catastrophic floods on Mars and Earth. Icarus 1974;23:27–41. doi:10.1016/0019-1035(74)90101-8.
[6] Bargery AS, Wilson L. Erosive flood events on the surface of Mars: application to Mangala and Athabasca Valles. Icarus 2011;212:520–40. doi:10.1016/j.icarus.2011.01.001.
[7] Bense V, Gleeson T, Loveless S, Bour O, Scibek J. Fault zone hydrogeology. Earth Sci Rev 2013;127:171–92. doi:10.1016/j.earscirev.2013.09.008.
[8] Cabrol N, Grin EA, Dawidowicz G. A model of outflow generation by hydrothermal underpressure drainage in volcano-tectonic environment, Shalbatana Vallis (Mars). Icarus 1997;125:455–64. doi:10.1006/icar.1996.5625.
[9] Carr MH. Formation of Martian flood features by release of water from confined aquifers. J Geophys Res 1979;84:2995–3007. doi:10.1029/JB084iB06p02995.
[10] Carr MH. The Martian drainage system and the origin of valley networks and fretted channels. J Geophys Res 1995;100:7479. doi:10.1029/95JE00260.
[11] Carr MH. Elevations of water-worn features on Mars: implications for circulation of groundwater. J Geophys Res 2002;107:5131. doi:10.1029/2002JE001845.
[12] Chapman MG, Gudmundsson MT, Russell AJ, Hare TM. Possible Juventae Chasma subice volcanic eruptions and Maja Valles ice outburst floods on Mars: implications of Mars Global Surveyor crater densities, geomorphology, and topography. J Geophys Res 2003;108:5113. doi:10.1029/2002JE002009.
[13] Christensen PR, Jakosky BM, Kieffer HH, Malin MC, McSweenJr HY, Nealson K, et al. The Thermal Emission Imaging System (THEMIS) for the Mars 2001 Odyssey Mission. Space Sci Rev 2004;110:85–130. doi:10.1023/B:SPAC.0000021008.16305.94.
[14] Clifford SM. A model for the hydrologic and climatic behavior of water on Mars. J Geophys Res 1993;98:10973. doi:10.1029/93JE00225.
[15] Clifford SM, Parker TJ. The evolution of the Martian hydrosphere: implications for the fate of a primordial ocean and the current state of the northern plains. Icarus 2001;154:40–79. doi:10.1006/icar.2001.6671.
[16] Coleman NM. Hydrographs of a Martian flood from a breached crater lake, with insights about flow calculations, channel erosion rates, and chasma growth. J Geophys Res Planets 2013;118:263–77. doi:10.1029/2012JE004193.
[17] Coleman NM, Dinwiddie CL, Casteel K. High outflow channels on Mars indicate Hesperian recharge at low latitudes and the presence of Canyon Lakes. Icarus 2007;189:344–61. doi:10.1016/j.icarus.2007.01.020.
[18] Conway SJ, Lamb MP, Balme M, Towner MC, Murray JB. Enhanced runout and erosion by overland flow at low pressure and sub-freezing conditions: experiments and application to Mars. Icarus 2011;211:443–57. doi:10.1016/j.icarus.2010.08.026.
[19] Dobry R, Ladd RS, Yokel FY, Chung RM, Powell D. Prediction of pore water pressure buildup and liquefaction of sands during earthquakes by the cyclic strain method. Washington, DC: U.S. Department of Commerce, National Bureau of Standards; 1982.
[20] Fergason R, Lee EM, Weller L. THEMIS geodetically controlled mosiacs of Mars. 44th Lunar and Planetary Science Conference. The Woodlands, Texas; 2013. abstract 1642.
[21] Fergason RL, Christensen PR, Kieffer HH. High-resolution thermal inertia derived from the Thermal Emission Imaging System (THEMIS): thermal model and applications. J Geophys Res E Planets 2006;111:1–22. doi:10.1029/2006JE002735.
[22] Flahaut J, Mustard JF, Quantin C, Clenet H, Allemand P, Thomas P. Dikes of distinct composition intruded into Noachian-aged crust exposed in the walls of Valles Marineris. Geophys Res Lett 2011;38. doi:10.1029/2011GL048109.
[23] Fueten F, Flahaut J, Stesky R, Hauber E, Rossi AP. Stratigraphy and mineralogy of Candor Mensa, West Candor Chasma, Mars: insights into the geologic history of Valles Marineris. J Geophys Res Planets 2014;119:331–54. doi:10.1002/2013JE004557.
[24] Hanna JC, Phillips RJ. Hydrological modeling of the Martian crust with application to the pressurization of aquifers. J Geophys Res 2005;110:E01004. doi:10.1029/2004JE002330t.
[25] Hanna JC, Phillips RJ. Tectonic pressurization of aquifers in the formation of Mangala and Athabasca Valles, Mars. J Geophys Res 2006;111:E03003. doi:10.1029/2005JE002546.
[26] Harrison KP, Chapman MG. Evidence for ponding and catastrophic floods in central Valles Marineris, Mars. Icarus 2008;198:351–64. doi:10.1016/j.icarus.2008.08.003.
[27] Harrison KP, Grimm RE. Tharsis recharge: a source of groundwater for Martian outflow channels. Geophys Res Lett 2004;31:L14703. doi:10.1029/2004GL020502.
[28] Harrison KP, Grimm RE. Regionally compartmented groundwater flow on Mars. J Geophys Res 2009;114:E04004. doi:10.1029/2008JE003300.
[29] Hartmann WK, Neukum G. Cratering chronology and the evolution of Mars. Space Sci Rev 2001;96:165–94. doi:10.1023/A:1011945222010.
[30] Head JW, Wilson L, Mitchell KL. Generation of recent massive water floods at Cerberus Fossae, Mars by dike emplacement, cryospheric cracking, and confined aquifer groundwater release. Geophys Res Lett 2003;30:1577. doi:10.1029/2003GL017135.
[31] de Hon RA, Pani EA. Duration and rates of discharge: Maja Valles, Mars. J Geophys Res 1993;98:9129. doi:10.1029/93JE00535.
[32] Irwin RP, Maxwell TA, Howard AD, Craddock RA, Leverington DW. A large paleolake basin at the head of Ma'adim Vallis, Mars. Science 2002;296:2209–12. doi:10.1126/science.1071143.
[33] Jaumann R, Neukum G, Behnke T, Duxbury T, Eichentopf K, Flohrer J, et al. The high-resolution stereo camera (HRSC) experiment on Mars Express: instrument aspects and experiment conduct from interplanetary cruise through the nominal mission. Planet Space Sci 2007;55:928–52. doi:10.1016/j.pss.2006.12.003.
[34] Komatsu G, Di Achille G, Popa C, Di Lorenzo S, Rossi AP, Rodríguez JAP. Paleolakes, paleofloods, and depressions in Aurorae and Ophir Plana, Mars: connectivity of surface and subsurface hydrological systems. Icarus 2009;201:474–91. doi:10.1016/j.icarus.2009.01.010.
[35] Lasue J, Mangold N, Hauber E, Clifford S, Feldman W, Gasnault O, et al. Quantitative assessments of the Martian hydrosphere. Space Sci Rev 2013;174:155–212. doi:10.1007/s11214-012-9946-5.
[36] Leask HJ, Wilson L, Mitchell KL. Formation of Ravi Vallis outflow channel, Mars: morphological development, water discharge, and duration estimates. J Geophys Res 2006;111:E08070. doi:10.1029/2005JE002549.
[37] Leverington DW. A volcanic origin for the outflow channels of Mars: key evidence and major implications. Geomorphology 2011;132:51–75. doi:10.1016/j.geomorph.2011.05.022.

[38] Lucchitta BK. Lakes in Valles Marineris. Lakes on Mars. Elsevier B.V.; 2010. p. 111–61. doi:10.1016/B978-0-444-52854-4.00005-2.
[39] Malin MC, Bell JF, Cantor BA, Caplinger MA, Calvin WM, Clancy RT, et al. Context Camera Investigation on board the Mars Reconnaissance Orbiter. J Geophys Res 2007;112:E05S04. doi:10.1029/2006JE002808.
[40] Marra WA, Braat L, Baar AW, Kleinhans MG. Valley formation by groundwater seepage, pressurized groundwater outbursts and crater-lake overflow in flume experiments with implications for Mars. Icarus 2014;232:97–117. doi:10.1016/j.icarus.2013.12.026.
[41] Marra WA, Hauber E, McLelland SJ, Murphy BJ, Parsons DR, Conway SJ, et al. Pressurized groundwater outflow experiments and numerical modeling for outflow channels on Mars. J Geophys Res Planets 2014;119:2668–93. doi:10.1002/2014JE004701.
[42] Michael G. Planetary surface dating from crater size-frequency distribution measurements: multiple resurfacing episodes and differential isochron fitting. Icarus 2013;226:885–90. doi:10.1016/j.icarus.2013.07.004.
[43] Michaut C, Baratoux D, Thorey C. Magmatic intrusions and deglaciation at mid-latitude in the northern plains of Mars. Icarus 2013;225:602–13. doi:10.1016/j.icarus.2013.04.015.
[44] Milana JP. The sieve lobe paradigm: observations of active deposition. Geology 2010;38:207–10. doi:10.1130/G30504.1.
[45] Neukum G, Basilevsky AT, Kneissl T, Chapman M, van Gasselt S, Michael G, et al. The geologic evolution of Mars: episodicity of resurfacing events and ages from cratering analysis of image data and correlation with radiometric ages of Martian meteorites. Earth Planet Sci Lett 2010;294:204–22. doi:10.1016/j.epsl.2009.09.006.
[46] Paola C, Straub K, Mohrig D, Reinhardt L. The unreasonable effectiveness of stratigraphic and geomorphic experiments. Earth Sci Rev 2009;97:1–43. doi:10.1016/j.earscirev.2009.05.003.
[47] Presley MA, Christensen PR. The effect of bulk density and particle size sorting on the thermal conductivity of particulate materials under Martian atmospheric pressures. J Geophys Res 1997;102:9221. doi:10.1029/97JE00271.
[48] Quantin C, Allemand P, Mangold N, Dromart G, Delacourt C. Fluvial and lacustrine activity on layered deposits in Melas Chasma, Valles Marineris, Mars. J Geophys Res 2005;110:E12S19. doi:10.1029/2005JE002440.
[49] Roda M, Kleinhans MG, Zegers TE, Oosthoek JH. Aram Chaos: evidence for catastrophic ice lake collapse on Mars. Icarus 2014;236:104–21. doi:10.1016/j.icarus.2014.03.023.
[50] Rodríguez JAP, Gulick VC, Baker VR, Platz T, Fairén AG, Miyamoto H, et al. Evidence for Middle Amazonian catastrophic flooding and glaciation on Mars. Icarus 2014;242:202–10. doi:10.1016/j.icarus.2014.06.008.
[51] Rodríguez JAP, Sasaki S, Miyamoto H. Nature and hydrological relevance of the Shalbatana complex underground cavernous system. Geophys Res Lett 2003;30:1304. doi:10.1029/2002GL016547.
[52] Russell PS, Head JW. Elysium-Utopia flows as mega-lahars: a model of dike intrusion, cryosphere cracking, and water-sediment release. J Geophys Res 2003;108:5064. doi:10.1029/2002JE001995.
[53] Sato H, Kurita K, Baratoux D. The formation of floor-fractured craters in Xanthe Terra. Icarus 2010;207:248–64. doi:10.1016/j.icarus.2009.10.023.
[54] Scholten F, Gwinner K, Roatsch T, Matz KD, Wählisch M, Giese B, et al. Mars Express HRSC data processing-methods and operational aspects. Photogramm Eng Remote Sens 2005;71:1143–52. doi:10.14358/PERS.71.10.1143.
[55] Schultz RA. Multiple-process origin of Valles Marineris basins and troughs, Mars. Planet Space Sci 1998;46:827–34. doi:10.1016/S0032-0633(98)00030-0.
[56] Schultz RA. Localization of bedding plane slip and backthrust faults above blind thrust faults: keys to wrinkle ridge structure. J Geophys Res 2000;105:12035. doi:10.1029/1999JE001212.
[57] Spencer JR, Fanale FP. New models for the origin of Valles Marineris closed depressions. J Geophys Res 1990;95:14301. doi:10.1029/JB095iB09p14301.
[58] Tanaka KL, Skinner JA, Dohm JM, RP Irwin I, Kolb EJ, Fortezzo CM, et al. Geologic map of Mars: U.S. Geological Survey Scientific Investigations Map 3292, scale 1:20,000,000. pamphlet; 2014, doi:10.3133/sim3292.
[59] Voelker M, Platz T, Tanaka KL, Fortezzo CM, Fergason RL. Hyperconcentrated flow deposits and valley formation of Havel Vallis, Xanthe Terra, Mars. 44th Lunar and Planetary Science Conference, The Woodlands, Texas; 2013. abstract 2886.
[60] Voelker M, Platz T, Tanaka KL, Fortezzo CM, Fergason RL, Hare TM. Geological mapping of Havel Vallis, Xanthe Terra, Mars: stratigraphy and reconstruction of valley formation. 44th Lunar and Planetary Science Conference, The Woodlands, Texas; 2012. abstract 2738.
[61] Wang C, Manga M, Hanna JC. Can freezing cause floods on Mars? Geophys Res Lett 2006;33:L20202. doi:10.1029/2006GL027471.
[62] Wang C, Manga M, Wong A. Floods on Mars released from groundwater by impact. Icarus 2005;175:551–5. doi:10.1016/j.icarus.2004.12.003.
[63] Warner N, Gupta S, Muller JP, Kim JR, Lin SY. A refined chronology of catastrophic outflow events in Ares Vallis, Mars. Earth Planet Sci Lett 2009;288:58–69. doi:10.1016/j.epsl.2009.09.008.
[64] Warner NH, Sowe M, Gupta S, Dumke A, Goddard K. Fill and spill of giant lakes in the eastern Valles Marineris region of Mars. Geology 2013;41:675–8. doi:10.1130/G34172.1.
[65] Weitz CM, Noe Dobrea E, Wray JJ. Mixtures of clays and sulfates within deposits in western Melas Chasma, Mars. Icarus 2014. doi:10.1016/j.icarus.2014.04.009.
[66] Wilson L, Mouginis-Mark PJ. Dynamics of a fluid flow on Mars: lava or mud? Icarus 2014;233:268–80. doi:10.1016/j.icarus.2014.01.041.
[67] Wyrick D, Ferrill DA, Morris AP, Colton SL, Sims DW. Distribution, morphology, and origins of Martian pit crater chains. J Geophys Res 2004;109:E06005. doi:10.1029/2004JE002240.
[68] Zuber MT, Smith DE, Solomon SC, Muhleman DO, Head JW, Garvin JB, et al. The Mars Observer laser altimeter investigation. J Geophys Res 1992;97:7781. doi:10.1029/92JE00341.